This is the accepted manuscript of the article that appeared in final form in **Nuclear Instruments and Methods in Physics Research Section B** 258(1) : 72–78 (2007), which has been published in final form at https://doi.org/10.1016/j.nimb.2006.12.133. © 2007 Elsevier under CC BY-NC-ND license (http://creativecommons.org/licenses/by-nc-nd/4.0/)

Dynamic screening and electron dynamics in low-dimensional metal systems

V. M. Silkin [a], M. Quijada [a,b], M. G. Vergniory [a,c], M. Alducin [a], A. G. Borisov [a,d], R. Díez Muiño [a,e], J. I. Juaristi [a,b,e], D. Sánchez-Portal [a,e], E. V. Chulkov [a,b,e], P. M. Echenique [a,b,e]

[a] *Donostia International Physics Center DIPC, P. Manuel de Lardizabal 4, 20018 San Sebastián, Spain*

[b] *Departamento de Física de Materiales, Facultad de Químicas, UPV/EHU, Apartado 1072, 20080 San Sebastián, Spain*

[c] *Departamento de Física de la Materia Condensada, Facultad de Ciencia y Tecnología, UPV/EHU, Apartado 644, 48080 Bilbao, Spain*

[d] *Laboratoire des Collisions Atomiques et Moléculaires (UMR CNRS-Université Paris-Sud 8625), Bât. 351, Université Paris-Sud, 91405 Orsay Cedex, France*

[e] *Unidad de Física de Materiales, Centro Mixto CSIC-UPV/EHU, Apartado 1072, 20080 San Sebastián, Spain*

Abstract

Recent advances in the theoretical description of dynamic screening and electron dynamics in metallic media are reviewed. The time-dependent building-up of screening in different situations is addressed. Perturbative and non-perturbative theories are used to study electron dynamics in low-dimensional systems, such as metal clusters, image states, surface states, and quantum wells. Modification of the electronic lifetimes due to confinement effects is analyzed as well.

Key words:
Dynamic screening, Low-dimensional systems, Quasiparticles, Electron dynamics
PACS:

1 Introduction

The screening response to an external Coulomb field is a fundamental property of electronic media. Screening reduces the interaction range between charged particles and enhances locality in many processes. The understanding of screening is of paramount importance for the quantitative interpretation of many surface characterization methods, such as Auger spectroscopy, low-energy electron diffraction, and ion beam analysis. The interaction between the external charge and the target involves various phenomena. Among them, we quote electronic energy losses and charge exchange [1–5]. The theoretical description of these processes demands an adequate characterization of the screening response in the medium. Density functional theory (DFT) has been applied to study the embedding of atomic [6,7] and molecular [8,9] species in an electron gas. This model has been often used as a framework to study static screening properties. It has allowed, for instance, to study kinetic electron emission induced by slow ions [10] and potential electron emission induced by the Auger neutralization of ions in metals [11–13]. However, a proper treatment of *dynamic* screening is required to study the interaction of moving charges with solids, surfaces, and nanostructures.

Dynamic screening of electrons in an interacting Fermi liquid lies behind the concept of quasiparticle, one of the most useful models to describe theoretically electronic excitations [14]. The interaction between quasiparticles determines the time scales in which the corresponding quantum states retain their identity. A quasiparticle is said to have a lifetime, which sets the duration of the excitation. Furthermore, the lifetime determines the mean free path of the quasiparticle, a measure of the range of influence of the excitation. The quasiparticle lifetime is of relevance in the description of many important phenomena, such as the dynamics of charge and energy transfer, electron-phonon coupling, localization, quantum interference, and many others. Electronically excited states can act as intermediate steps in various chemical processes. Either enhancement or reduction of the reaction rate should be thus possible through a proper design of the intermediate step lifetime.

In this article, we review recent advances in the theoretical description of dynamic screening and electron lifetimes in different situations. Both perturbative and non-perturbative models are presented. Particular attention is paid to the knowledge acquired for short timescales and/or low dimensional systems. In these two cases, general ideas commonly accepted for the dynamic screening in bulk can fail and new developments are necessary. For the short-time regime, TDDFT calculations in finite-sized systems show that the screening is built-up locally on a time scale well below the femtosecond for typical metallic densities. In this scale, the time evolution of the electron density is not affected by the system boundaries. Therefore, the conclusions drawn from the study of

finite-sized systems are valid for the infinite system as well. Universal scaling laws and dimensionality effects in the time-dependent screening of charges are discussed. For many other situations, the long-time dynamics of screening is needed: band structure effects in solids and boundary effects in finite systems can play and important role and significantly modify electron dynamics as compared with the FEG exemplary reference.

2 Building-up the screening in time

Let us first start with some general ideas about the time scale required to screen charges in a metallic medium. Indeed, the rearrangement of electronic charge needed for the screening is not instantaneous but develops in a finite time. In general, standard experimental techniques provide information over time scales for which the screening of charges can be approximated as instantaneous in practice, being much faster than any other measurable process. However, constant improvements in experimental methods, particularly in the field of ultrafast laser spectroscopies, are making it possible to access time scales for which the rearrangement of charge is dynamic and the screening is not complete [15,16]. Therefore, it is necessary to develop new theoretical approaches to understand how the screening is built-up in many-electron systems.

Let us use a simple model in which a point charge is suddenly created in a metallic medium. Both linear response theory (LRT) and time-dependent density functional theory (TDDFT) have shown to be valuable tools to calculate the characteristic short-time response of three-dimensional (3D) [17,18] and two-dimensional (2D) [19,20] free electron gases (FEG). The striking difference between the time evolution of the electron density in 2D and 3D in response to the sudden creation of a point charge q is the quick damping of collective excitations in 2D, and the durability of them in 3D (see Figs. 1 and 2). In 2D we observe that, behind the wave front propagating with velocity close to the Fermi velocity k_f, the electron density basically reaches the stationary limit. This includes the formation of the characteristic Friedel oscillations. Hence, the evolution of the electron density close to the probe q can be considered as over after ≈ 30 a.u. (i.e., ≈ 0.7 fs).

In general, the rearrangement of electron density induced by the appearance of a sudden Coulomb field in a 2D FEG reaches the stationary value in much shorter times than in 3D. The source of this dissimilarity is the different behavior of the plasmon dispersion in 2D [$\omega = (2k)^{1/2}/r_s$] and 3D ($\omega \approx \omega_p$) in the $k \to 0$ limit. Here ω is the excitation energy, ω_p the plasmon energy, and k the linear momentum. Oscillations of the electron density in the 2D FEG are rapidly damped due to interference among collective excitations with different

frequencies. In 3D, oscillations last for much longer times, as a consequence of the similarity among the frequencies of the contributing modes.

Both in 2D and 3D, our TDDFT calculations show that the screening hole is created over a time scale of ≈ 5 a.u. (i.e., ≈ 0.1 fs). The origin of this result lies in the general trends of the short-time dynamics in the many-body system. On time scales corresponding to the creation of the screening hole, electronic correlations do not play any significant role and the electron density evolves in time as if it would correspond to that built from independent particles. The order of magnitude of 0.1 fs is roughly kept over a wide range of realistic values of the electron density.

Transient effects in the screening also appear in other situations, such as the establishment of the image potential when an external charge approaches a surface [21]. The existence of the image potential leads to the formation of image states, which are electron states bound between the image potential and the surface barrier [22]. Image states have been the subject of active research in recent years [23,24]. Two different time scales can be defined in this situation: (i) the time required for the creation of the image potential and (ii) the time it takes to converge to its stationary value. For a typical metallic density at the surface, the order of magnitude of the creation time is ≈ 5 a.u. (≈ 0.1 fs). The convergence time is more difficult to characterize by a single value, because it increases with the distance at which the charge is created from the surface. For a charge created close to the surface it is of the order of few fs [21].

3 Electron dynamics in image states and image state resonances

We mentioned in the previous section that image states for excited electrons arise in front of a metal surface because of the interaction with the polarization charge that the electron produces at the surface. Far from the surface the interaction converges to the classical image potential $V(z) = -1/[4(z - z_{im})]$, where z_{im} is the position of the image plane. When the electron penetration into the metal is inhibited by a projected band gap, the image states are stationary within the one electron picture. They form a Rydberg series [22,25] with energy and linewidth proportional to n^{-2} and n^{-3}, respectively, n being the principal quantum number [26,22]. The decay of electrons excited into these states has been studied in detail both experimentally and theoretically [23,24]. It was shown that the main decay mechanism is the inelastic energy relaxation channel [23,24,27]. In this process, an image state electron undergoes interband transitions to unoccupied bulk and surface states of lower energy. The energy released in the process is transferred to electronic excitations. This is a many-body process in which dynamical bulk and surface screening

is implicitly included. An additional decay channel opens up when the electron momentum component parallel to the surface is finite ($k_{\|} \neq 0$). In this case, *intraband* transitions within the image state band can play an important role: around 50% of the increase of the image state linewidth is due to these transitions [28].

Another mechanism in the image states decay has recently been discussed, on the example of image-state resonances [29]. An image-state resonance is formed when the energy of the image state falls off the projected band gap of the surface. The electron can then be transferred from the image state to the continuum of bulk states through energy-conserving one-electron transfer. Hence the otherwise stationary (in a one-electron picture) image state is coupled to the continuum of states and becomes quasi-stationary, i.e., a resonance. Since one-electron transitions are more efficient than many-body ones, the resonant electron transfer is dominant for the image-state resonance decay.

A wave-packet propagation study of the one-electron resonant processes has allowed to obtain the lifetimes of image state resonances on the Cu(111) and Ag(111) surfaces in very good agreement with available time-resolved two-photon photoemission data [29,30]. In Fig. 3 we show the calculated dependence of the linewidth on the principal quantum number n for image resonance states on Cu(111), Ag(111), Au(111), and Be(0010). Similar to the gap image states [22], the linewidth of the image state resonances varies with n as n^{-3}. The n^{-3} dependence of the many-body width of the gap image states has been explained using penetration arguments [22]. However, for the image state resonances, the reason for the n^{-3} dependence is different and can be understood from quasi-classical arguments. Indeed, for the electron moving under action of the image potential and colliding from time to time with the surface, the rate of the electron escape into the metal is given by the fixed probability of transmission through the metal-vacuum interface multiplied by the collision frequency. Since the difference in energies of the image resonance states is relatively small, the transmission probability is basically constant through the n-series. The collision frequency is proportional to n^{-3}, as can be inferred from the period of the Rydberg electron motion in the Coulomb field. Therefore, the resulting width has a n^{-3} dependence.

4 Electron dynamics in metal clusters

As compared to the bulk counterpart, confinement effects in metal clusters and nanoparticles affect the lifetime of electronic excitations in two different aspects: (i) the density of states varies and clear resonances appear in the valence band excitation spectrum as the cluster size decreases, and (ii) screening between electrons is less efficient, both at the surface and inside the cluster.

In principle, these two effects act in opposite directions, as the former should increase the lifetime and the latter should shorten it. For this reason, metal clusters appear as promising systems for which an adequate choice of material and size may allow to tune at wish the lifetime of electron excitations.

The dependence on system-size of the electron-electron interaction processes has been studied experimentally using techniques based on femtosecond lasers [31–34]. Some of the conclusions extracted from these works are puzzling. Voisin *et al.* showed that the electron-electron scattering rate (i.e., the inverse of the electron-electron lifetime) is increased for Ag nanoparticles of size smaller than 5 nm, as compared with the bulk reference value [31]. This modification was attributed to the induced reduction of the Coulomb interaction screening at the nanoparticle surface [31]. However, Merschdorf *et al.* measured electron lifetimes in supported Ag nanoparticles appreciably higher than those obtained for Ag bulk or Ag films [34]. These apparently contradictory conclusions show the necessity of further research on the subject.

Theoretical calculations based on the spherical jellium model for the cluster and on the GW approximation show that the lifetime τ_{e-e} of electronic excitations with energy $E_o \approx 1$ eV above the Fermi level are of the order of a few fs. [35]. In Fig. 4, τ_{e-e} is plotted as a function of the cluster radius R. For small cluster sizes, the discretization of energy levels is clearly observable in the large oscillations found. However, these oscillations are damped for clusters of nanometer size and the value of the lifetime is $\tau_{e-e} \approx 4$ fs. In a homogeneous electron gas, a similar calculation of the electron lifetime with $E_o = 1$ eV and $r_s = 4$ gives a value $\tau_{e-e} = 11$ fs. This is longer than the one obtained for the biggest clusters shown here.

5 Electron dynamics in quantum well states

Under the deposition of alkali atoms on metal surfaces, quantum well states appear [36,37]. Whereas the number of adsorbed alkali atoms is small, the alkali atoms can be considered as independent. Under these conditions, the picture of almost total transfer of s valence electron from the alkali atom to the substrate is appropriate. However, when the coverage reaches rates of around 1 monolayer (ML) [38], an adsorbate-induced electron band [called a Quantum Well State (QWS)] forms a quasi two-dimensional electron gas. The QWS is confined between the vacuum barrier and the metal substrate [39,40]. This band, which is unoccupied for lower coverage, starts to fill for higher coverages[41]. A prominent example of such a system is the case of Na adsorption on Cu(111), for which the properties of the quantum well state have been intensively studied. For instance, the dynamics of holes of wave vector $k_{\|} = 0$ has been studied for Na/Cu(111), both experimentally and

theoretically [42]. For 1 ML coverage, it was proven that the *e*-*e* and the *e*-*ph* mechanisms are equally important for the hole decay. *Intraband* transitions within the QWS itself account for 98% of the total *e*-*e* contribution to the QWS hole linewidth. This value is even larger than on clean Cu(111) surface, where intraband transitions within the surface state band account for 85% of the total *e*-*e* contribution [43]. Very recently, a joint experimental and theoretical study of electron dynamics for Cs and Na adlayers on Cu(111) has been performed as well [44]. This work shows the growing importance of the elastic or resonant tunnelling contribution to the lifetime of the QWS as the coverage is reduced. For the Na and Cs 2x2 overlayers, this elastic contribution accounts for almost a 50% of the measured linewidth for the unoccupied QWS at $\bar{\Gamma}$.

In Na/Cu(111), the modification in the alkali atoms coverage leads to a shift of the QWS energy band. This shift produces an appreciable change in the linewidth Γ_{e-e}. This is shown in Fig. 5, in which the calculated dependence of Γ_{e-e} on the excited energy is presented for three Na QWS energy positions. The behavior of Γ_{e-e} as a function of the QWS energy position can be understood with the help of Figs. 6 and 7. In these figures, the imaginary part of the screened interaction $\mathrm{Im}W(z, z, q_{\|}, \omega)$ is plotted as a function of z and ω for $E_{\bar{\Gamma}}^{QWS}$=−0.127 eV $E_{\bar{\Gamma}}^{QWS}$=0 eV, and for two-dimensional momenta $q_{\|} = 0.05$ $a.u.^{-1}$ and $q_{\|} = 0.10$ $a.u.^{-1}$. These figures show that ImW is much larger for the partially occupied QWS case than for the unoccupied QWS case.

6 Ultrafast electron dynamics at adsorbates

Electron dynamics is often investigated by means of laser pump-probe techniques, in which a pump pulse excites the system of interest and a second probe pulse tracks its temporal evolution. The time resolution attainable in such experiments depends on the temporal definition of the laser pulses. Because of this, pulse compression to 200 as is a promising recent development. These ultrafast pulses have been fully characterized and used to directly measure light waves and electronic relaxation in free atoms [15,16]. But attosecond pulses can only be realized in the extreme ultraviolet and X-ray regime. In contrast, the optical laser pulses typically used for experiments on complex systems last as much as several fs. For this reason, monitoring the dynamics of ultrafast electron transfer on attosecond timescales requires the help of core-hole spectroscopy: the lifetime of a core electron hole can be used as an internal reference clock for following dynamic processes [45,46]. This methodology does not require the use of ultrafast laser pulses. Synchrotron light sources are used instead. By focusing on short-lived holes with initial and final states in the same electronic shell, one can show that electron transfer from an adsorbed sulphur atom to a ruthenium surface proceeds in about 320 as [47].

First-principles methods can be of much help in the calculation of charge transfer times from electronically excited adsorbates to the substrate. For example, computations of the charge-transfer dynamics performed in the c(4×2)S/Ru(0001) system show that the excitation into a resonance with predominantly $3p_z$ character yields a charge transfer time of 0.63 ± 0.15 fs [Fig. 8(b)]. When comparing experiment to theory, the theoretical time constant confirms that the charge transfer process takes place well below a femtosecond timescale. In particular, the comparison with the experimental value of 0.32 ± 0.09 fs is satisfactory, taking into account that the core vacancy is not described explicitly in the theoretical ground state calculation. Furthermore, the theoretical resonance position at 2 eV above the Fermi level is shifted with respect to the experimental absorption resonance, which is at 1.68 ± 0.1 eV above the Fermi level. The theory predicts a detailed dependence of the charge transfer time on the symmetry of the initial excited state. This can be translated into a dependence with the polarization of the excitation light as schematically indicated in Fig. 8 (a). For excitation into $3p_x$ or $3p_y$-like resonances (in plane) [Fig. 8(b)] with a smaller overlap to the substrate, a significantly larger charge transfer time of up to 1.15 ± 0.15 fs is obtained in the calculation. This theoretical result shows that different polarizations of the light favour different initial excited states, with different symmetries and overlaps with the states of the substrate, thus leading to different transfer times.

7 Summary and outlook

In this paper, we have reviewed recent developments in the theoretical understanding of the dynamic screening and lifetimes of quasiparticles in different situations. An important question to be addressed in these problems is to what extent screening transients can be neglected and long time dynamics of screening is accurate enough to describe the processes. We have shown that in most cases, this approximation is valid because one deals with typical time scales above the femtosecond, whereas screening transients are important at time scales below the femtosecond. Neverheless, we stress that novel experimental methods, such as ultrafast laser spectroscopies, are starting to explore the time scale for which screening transients can play a role.

Finally, we end up by noting that the study of short time scales can be achieved both by perturbative linear response methods and non-perturbative TDDFT. The latter approach is necessary when dealing with strongly perturbed systems such as those that one encounters in the case of ions interacting with solid matter. This suggests that the technique opens a gate to further applications such as the treatment of the energy loss of ions in solids within a single method applicable in all the range of velocities, or the study of Auger neutralization of ions in metals beyond the usual perturbative Fermi Golden Rule approach.

8 Acknowledgements

We acknowledge partial support by the University of the Basque Country UPV/EHU (Grant No. 9/UPV 00206.215-13639/2001), and the Spanish MCyT (Grant No. FIS2004-06490-CO3-00).

References

[1] T. L. Ferrell, R. H. Ritchie, Phys. Rev. B **16** (1977) 115.

[2] N. R. Arista, Phys. Rev. B **18** (1978) 1.

[3] P. M. Echenique, I. Nagy, A. Arnau, Int. J. Quant. Chem. **23** (1989) 521.

[4] A. Narmänn, R. Monreal, P.M. Echenique, F. Flores, W. Heiland, S. Schubert, Phys. Rev. Lett. **64** (1990) 1601.

[5] I. Nagy, B. Apagyi, K. Ladanyi, Phys. Rev. A **42** (1990) 1806.

[6] C. O. Almbladh, U. von Barth, Z. D. Popovic, M. J. Stott, Phys. Rev. B **14** (1976) 2250.

[7] E. Zaremba, L. M. Sander, H. B. Shore, J. H. Rose, J. Phys. F **7** (1977) 1763.

[8] R. Díez Muiño, A. Salin, Phys. Rev. B **60** (1999) 2074.

[9] R. Díez Muiño, A. Salin, Phys. Rev. B **62** (2000) 5207.

[10] J. I. Juaristi, M. Rösler, F. J. García de Abajo, Phys. Rev. B **58** (1998) 15838.

[11] M. Alducin, R. Díez Muiño, J. I. Juaristi, Phys. Rev. A **70** (2004) 012901.

[12] M. Alducin, R. Díez Muiño, J. I. Juaristi, A. Arnau, J. Electron Spectrosc. Relat. Phenom. **137** (2004) 401.

[13] M. Alducin, J. I. Juaristi, R. Díez Muiño, M. Rösler, P. M. Echenique, Phys. Rev. A **72** (2005) 024901.

[14] D. Pines, P. Nozières, *The Theory of Quantum Liquids*, Benjamin, New York, 1966.

[15] A. Baltuška, Th. Udem, M. Ulberacker, M. Hentschel, E. Goullelmakis, Ch. Gohle, R. Holzwarth, V.S. Yakovlev, A. Scrinzi, T.W. Hänsch, F. Krausz, Nature **421** (2003) 611.

[16] M. Drescher, M. Henschel, R. Kienberger, M. Uiberacker, V. Yakovlev, A. Scrinzi, Th. Westerwalbesloh, U. Kleineberg, U. Heinzmann, F. Krausz, Nature **419** (2002) 803.

[17] G.S. Canright, Phys. Rev. B **38** (1988) 1647.

[18] A. Borisov, D. Sánchez-Portal, R. Díez Muiño, P. M. Echenique, Chem. Phys. Lett. **387** (2004) 95.

[19] M. Alducin, J.I. Juaristi, P.M. Echenique, Surf. Sci. **559** (2004) 233.

[20] A. G. Borisov, D. Sánchez-Portal, R. Díez Muiño, P. M. Echenique, Chem. Phys. Lett. **393** (2004) 132.

[21] M. Alducin, R. Díez Muiño, J. I. Juaristi, J. Electron Spectrosc. Relat. Phenom. **129** (2003) 105.

[22] P. M. Echenique, J. B. Pendry, J. Phys. C **11** (1978) 2065.

[23] P. M. Echenique, R. Berndt, E. V. Chulkov, Th. Fauster, A. Goldmann, U. Höfer, Surf. Sci. Rep. **52** (2004) 219.

[24] E. V. Chulkov, A. G. Borisov, J. P. Gauyacq, D. Sánchez-Portal, V. M. Silkin, V. P. Zhukov, P. M. Echenique, Chem. Rev. **106** (2006) 4160.

[25] E. V. Chulkov, V. M. Silkin, P. M. Echenique, Surf. Sci. **437** (1999) 330.

[26] U. Höfer, I. L. Shumay, Ch. Reuß, U. Thomann, W. Wallauer, Th. Fauster, Science **277** (1997) 1480.

[27] E. V. Chulkov, I. Sarría, V. M. Silkin, J. M. Pitarke, P. M. Echenique, Phys. Rev. Lett. **80** (1998) 4947.

[28] W. Berthold, U. Höfer, P. Feulner, E. V. Chulkov, V. M. Silkin, P. M. Echenique, Phys. Rev. Lett. **88** (2002) 056805.

[29] A. G. Borisov, E. V. Chulkov, P. M. Echenique, Phys. Rev. B **73** (2006) 073402.

[30] M. Weinelt, J. Phys.: Condens. Matter **14** (2002) R1099.

[31] C. Voisin, D. Christofilos, N. Del Fatti, F. Vallée, B. Prével, E. Cottancin, J. Lermé, M. Pellarin, M. Broyer, Phys. Rev. Lett. **85** (2000) 2200.

[32] N. Pontius, G. Lüttgens, P. S. Bechtold, M. Neeb, W. Eberhardt, J. Chem. Phys. **115** (2001) 10479.

[33] P. Gerhardt, M. Niemietz, Y. Dok Kim, and G. Ganteför, Chem. Phys. Lett. **382** (2003) 454.

[34] M. Merschdorf, C. Kennerknecht, W. Pfeiffer, Phys. Rev. B **70** (2004) 193401.

[35] M. Quijada, R. Díez Muiño, P. M. Echenique, Nanotechnology **16** (2005) 176.

[36] H. P. Bonzel, A. M. Bradshaw, G. Ertl, *Physics and Chemistry of Alkali Metal Adsorption*, Elsevier, Amsterdam, 1989.

[37] R. D. Diehl, R. McGrath, Surf. Sci. Rep. **23** (1996) 43.

[38] We define one Na monolayer as the most densly packed structure of the first Na layer, namely a $(3/2 \times 3/2)$ unit mesh with 4 Na atoms per 9 Cu surface atoms [D. Tang, D. McIlroy, X. Shi, C. Su, D. Heskett, Surf. Sci. **255** (1991) L497; J. Kliewer, R. Berndt, Surf. Sci. **477** (2001) 250].

[39] S.-Å. Lindgren, L. Walldén, Solid State Commun. **34** (1980) 671.

[40] S.-Å. Lindgren, L. Walldén, Phys. Rev. Lett. **59** (1987) 3003.

[41] N. Fischer, S. Schuppler, Th. Fauster, W. Steinmann, Surf. Sci. **314** (1994) 89.

[42] E. V. Chulkov, J. Kliewer, R. Berndt, V. M. Silkin, B. Hellsing, S. Crampin, P. M. Echenique, Phys. Rev. B **68** (2003) 195422.

[43] J. Kliewer, R. Berndt, E. V. Chulkov, V. M. Silkin, P. M. Echenique, S. Crampin, Science **288** (2000) 1399.

[44] C. Corriol, V. M. Silkin, D. Sánchez-Portal, A. Arnau, E. V. Chulkov, P. M. Echenique, T. von Hofe, J. Kliewer, J. Kröger, R. Bernd, Phys. Rev. Lett. **95** (2005) 176802.

[45] W. Wurth, D. Menzel, Chem. Phys. **251** (2000) 141.

[46] P. A. Brühwiler, O. Karis, N. Mårtensson, Rev. Mod. Phys. **74** (2002) 703.

[47] A. Föhlisch, P. Feulner, F. Hennies, A. Fink, D. Menzel, D. Sánchez-Portal, P. M. Echenique, W. Wurth, Nature **436** (2005) 373.

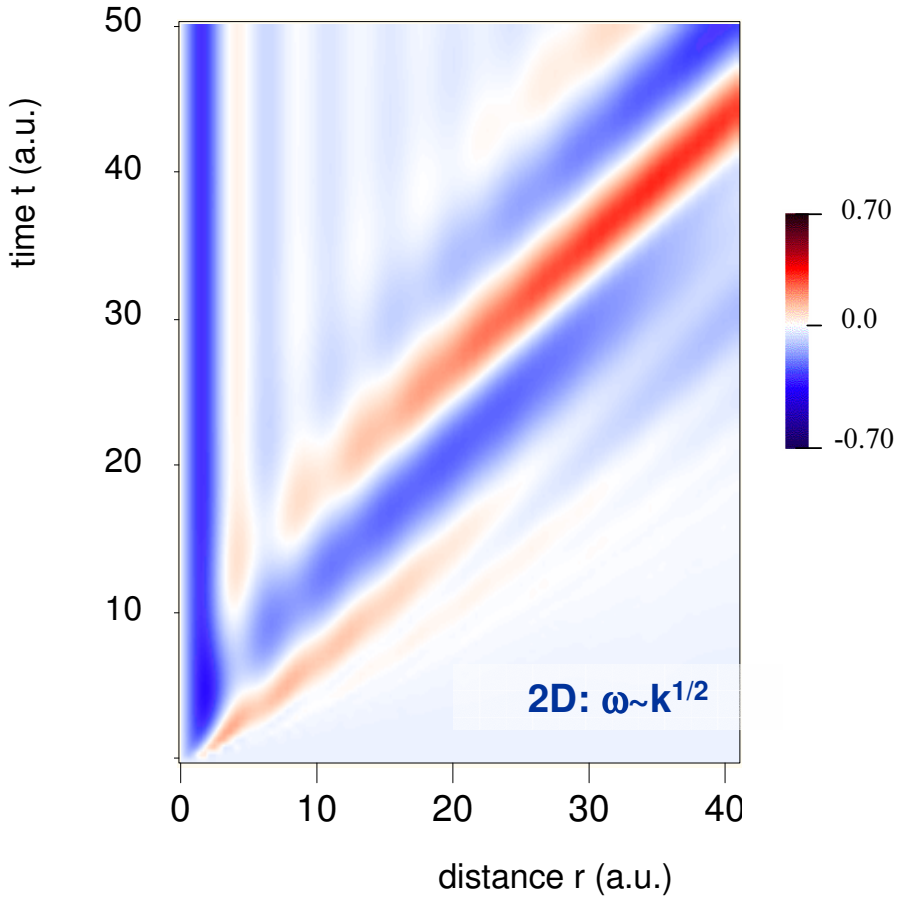

Fig. 1. Interpolated image of the time evolution of the radial induced electron density $\Delta q(r,t)$ when a charge $q=-1$ is introduced at $t=0$ at the center of a 2D jellium disk. The radius of the disk is $R_d=253$ and $r_s=2$. The induced charge is plotted as a function of time t (vertical axis) and radial distance from the center of the system r (horizontal axis). All quantities in atomic units.

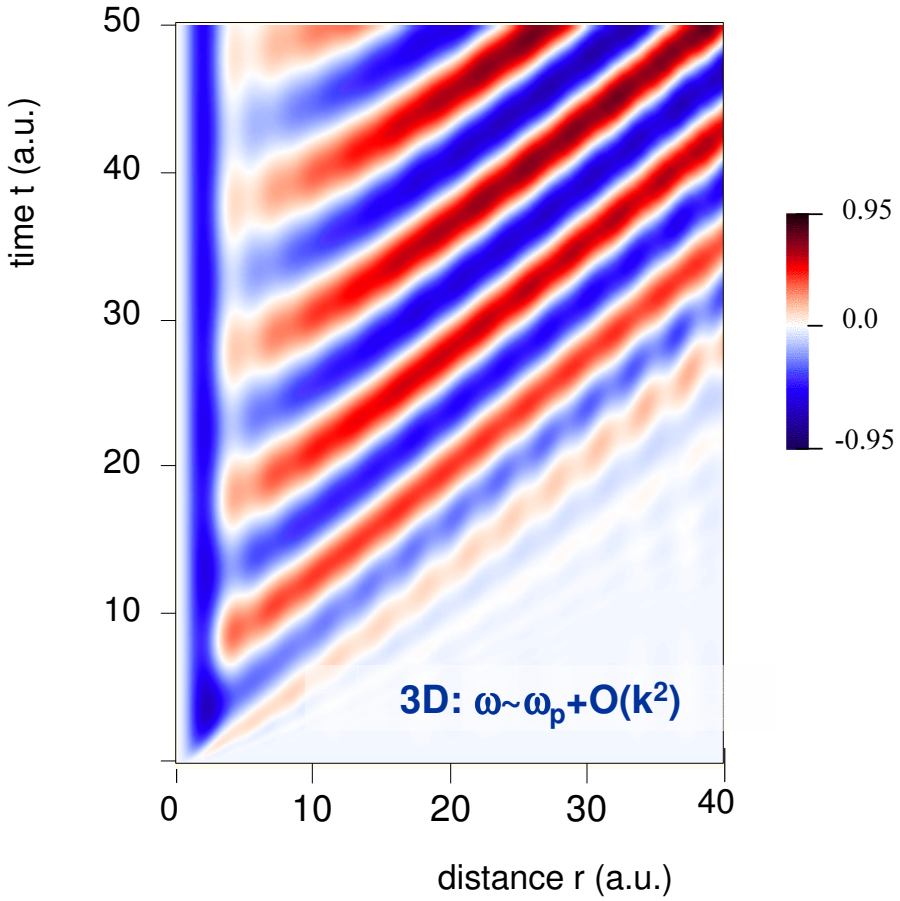

Fig. 2. Interpolated image of the time evolution of the radial induced electron density $\Delta q(r,t)$ when a charge $q=-1$ is introduced at $t=0$ at the center of a 3D jellium cluster. The radius of the cluster is $R_d=54.3$ and $r_s=2$. The induced charge is plotted as a function of time t (vertical axis) and radial distance from the center of the system r (horizontal axis). All quantities in atomic units.

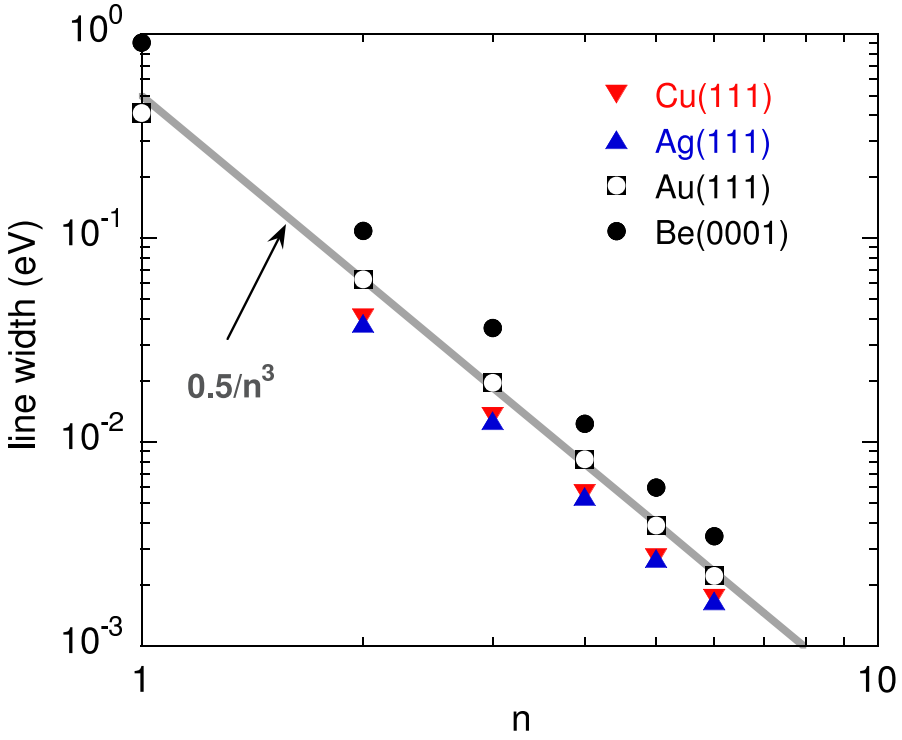

Fig. 3. Calculated linewidths of image state resonances as a function of the principal quantum number n for Cu(111), Ag(111), Au(111), and Be(0001). The logarithmic scale is used for both axes. The straight line traces the $0.5n^{-3}$ function to guide the eye.

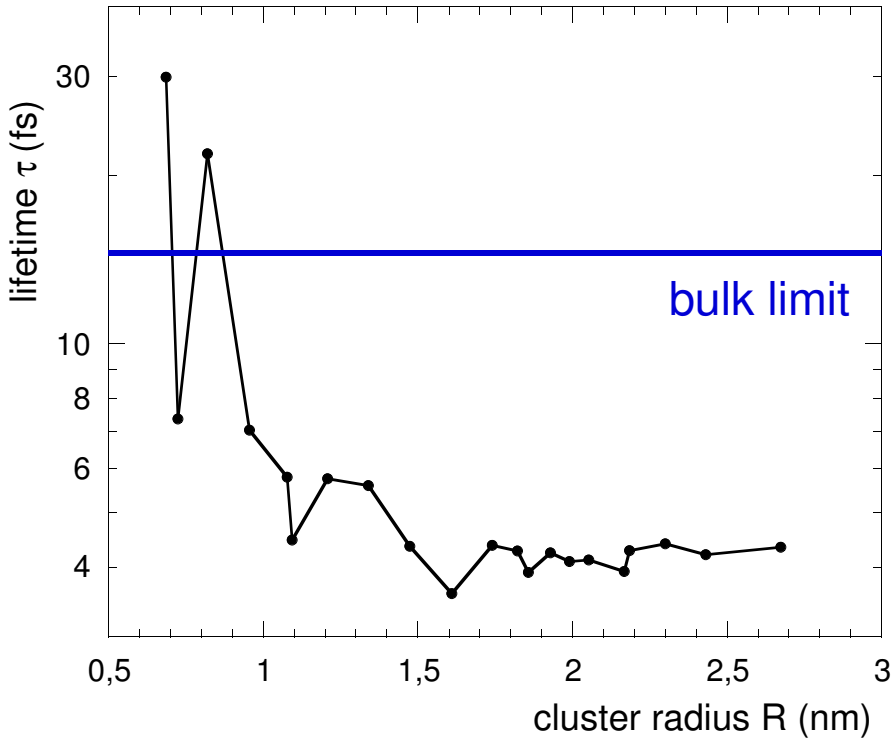

Fig. 4. Linewidth (in meV) of electron excitations with energy $E_0 \sim 1$ eV above the Fermi level of the cluster, as a function of the cluster radius (in a.u.). All systems have $r_s = 4$. The value of Γ_{e-e} obtained from an RPA calculation in an homogeneous electron gas with the same parameter r_s is also shown.

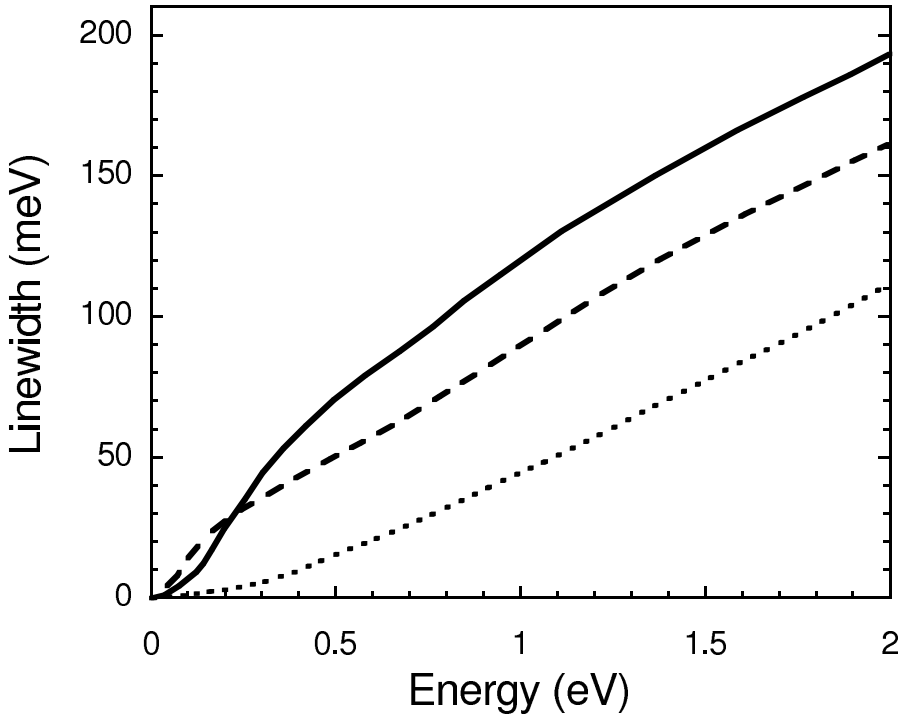

Fig. 5. Calculated *e*-*e* contribution, Γ_{e-e}, to the linewidth of a quantum well state in Na/Cu(111) for QWS energy position $E_{\overline{\Gamma}}^{QWS}$=−0.127 eV (solid line), $E_{\overline{\Gamma}}^{QWS}$=−0.042 eV (dashed line), and $E_{\overline{\Gamma}}^{QWS}$=0 (dotted line).

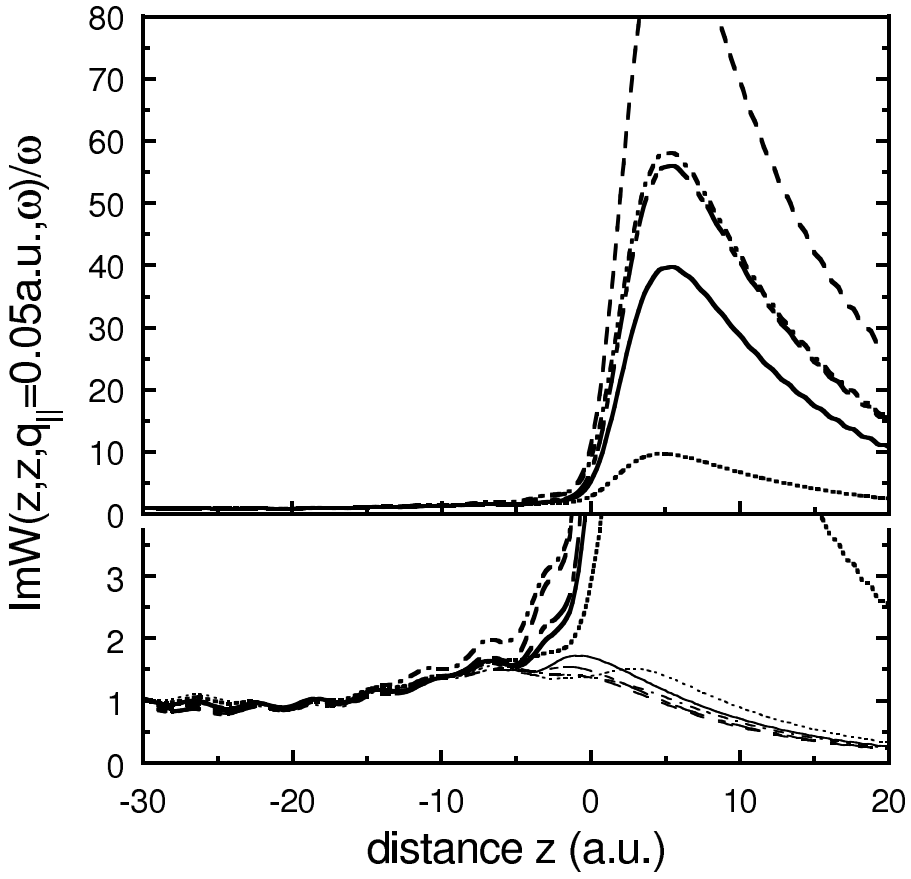

Fig. 6. Imaginary part of the screened interaction, $\mathrm{Im}W(z, z, q_{\|}, \omega)$, as a function of distance z and energy ω for the two-dimensional momentum $q_{\|} = 0.05\ a.u.^{-1}$. Na adlayer is located at $z = 0$ and negative (positive) z values correspond to the solid (vacuum) side. Upper panel shows $\mathrm{Im}W(z, z, q_{\|}, \omega)$ calculated for the $E_{\overline{\Gamma}}^{QWS}$=−0.127 eV case for $\omega = 0.06$ eV, 0.12 eV, 0.18 eV, 0.24 eV, and 0.30 eV (solid, long dashed, dashed, dashed-dotted, and dotted lines, respectively). Lower panel also includes $\mathrm{Im}W(z, z, q_{\|}, \omega)$ calculated for the $E_{\overline{\Gamma}}^{QWS}$=0 eV case (group of thin lines in a lower part of the panel).

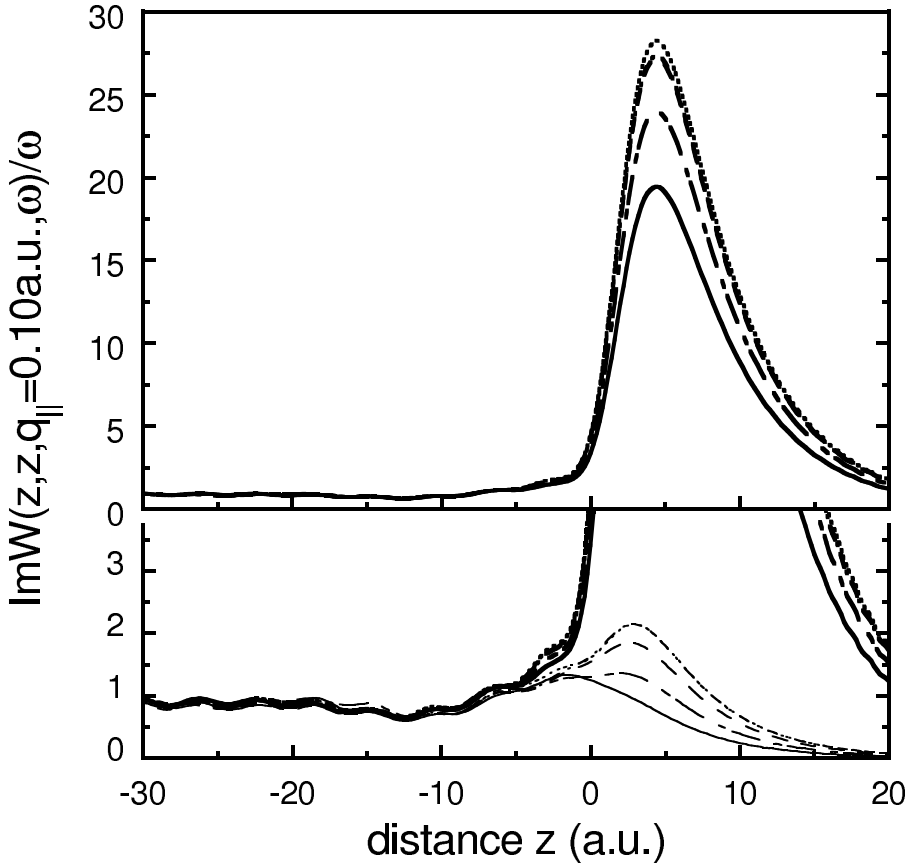

Fig. 7. Imaginary part of the screened interaction, $\mathrm{Im}W(z, z, q_{\|}, \omega)$, as a function of distance z and energy ω for the two-dimensional momentum $q_{\|} = 0.10\ a.u.^{-1}$. All notations as in Fig. 5.

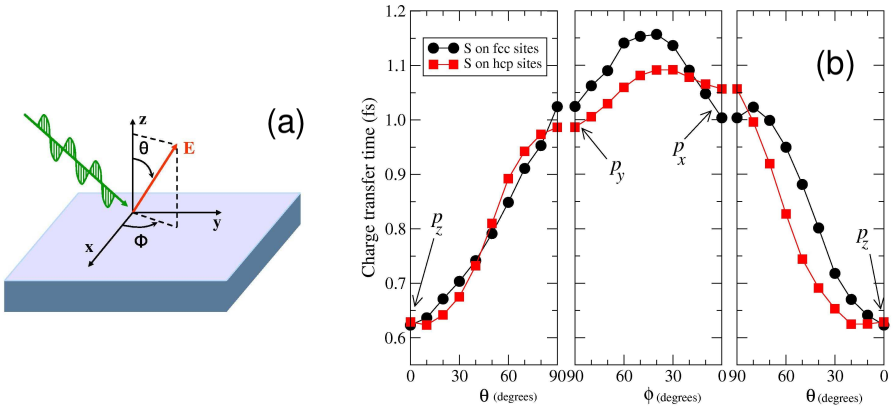

Fig. 8. Theory predicts a strong dependence of the charge transfer time on the symmetry of the initial wave packet, which translates into a strong dependence on the light polarization. The coordinates x, y, z shown in the diagram in (a) correspond to the crystallographic directions [100], [010], [001]. The scheme also indicates the angles formed by the polarization vector of light and these directions. Panel (b) shows the variation of the charge transfer time. The circles and squares correspond respectively to sulphur atoms in f.c.c. and h.c.p. sites of the surface. Polarization of the synchrotron light along the z axis (corresponding to the experimental geometry) produces an initial excited state with p_z symmetry and the shortest charge transfer time. Wavepackets with p_x and p_y symmetries and combinations of them are obtained with in-plane polarization.